

Time-Resolved Temperature Measurements in a Shock Tube Facility

S. O'Byrne¹, P. Altenhöfer² and A. Hohmann²

¹Department of Aerospace, Civil and Mechanical Engineering
University of New South Wales, Australian Defence Force Academy
Canberra, 2600, AUSTRALIA.

² Department of Aerospace Engineering, Universität Stuttgart, Stuttgart, GERMANY.

Abstract

This paper presents non-intrusive, time-resolved temperature measurements in the post-shock flow within a shock tube. We detail the technique, characterise its sensitivity to noise at various pressures, and present temperature measurements after the incident shock wave. Comparisons of experimental measurements with analytical correlations show good agreement with calculated post-shock temperatures at measurement rates of 1 kHz, but systematic errors occur at scan frequencies of 3 kHz, due to the limited bandwidth of our current detector system.

Introduction

Impulse facilities such as shock tubes and shock tunnels are challenging environments for measurements, due to regions of high temperature, pressure and velocity within typical flow fields. An additional challenge for quantitative measurement in these facilities involves the very short duration of the flow, ruling out many of the slower-response techniques commonly employed in wind-tunnel facilities. Non-intrusive, laser-based measurement techniques can potentially overcome all of these problems. These techniques have the additional advantage of being able to measure a number of different flow properties simultaneously. Against these advantages, laser-based techniques can be elaborate, expensive to assemble and difficult to maintain when compared with more traditional measurement techniques. There is thus a need for a simple, quantitative laser-based diagnostic that can be used to routinely measure the thermal characteristics of pulsed facility flows.

Many laser-based techniques have been employed in pulsed facilities. Planar laser-induced fluorescence (PLIF) has been successfully employed in shock tunnels for a number of applications, including characterisation of flow nonuniformities [11], for quantitative measurements of temperature [12], and for velocity using flow tagging [10] and measurement of Doppler shift [5]. Coherent anti-Stokes Raman scattering (CARS) has also been used for the measurement of temperature in these facilities [4]. Both of these spectroscopic techniques have two disadvantages limiting their wider application in pulsed facilities: they require complex, powerful, expensive lasers and their measurement rate is limited by the time between laser pulses, which is usually much greater than the facility flow duration. High-image-rate PLIF systems have been developed [15], although their expense currently makes them uncommon, and they have not yet been applied to impulse facilities.

Tuneable diode laser absorption spectroscopy (TDLAS) is a laser-based technique that has proved very popular for high-speed flow testing in recent years [1, 7]. Diode lasers can scan their wavelength at high frequency, require very little electrical power, have no moving parts and are much less expensive than the solid-state pump lasers and dye lasers used in PLIF and CARS experiments. The main disadvantage of diode-laser absorption-based techniques is that the measurement represents a weighted average of the conditions along the line of sight of

the laser beam, but where the conditions along the beam can be considered uniform TDLAS is well suited to high-speed flow measurements.

A number of diode-laser-based measurements have been performed in shock tunnels. Wehe *et al.* [18] made absorption measurements of temperature and water vapour concentration in the CUBRC LENS facility. Matsuda *et al.* [8] measured absorption of atomic oxygen in a free-piston shock tube by tuning the laser discretely over a number of facility runs and using the measured Doppler-broadened transition width to measure temperature, achieving qualitative agreement with computational predictions. Trinks and Beck [16] used absorption of seeded rubidium to measure temperature and velocity in a free-piston shock tunnel. More recently, Griffiths and Houwing [6] have measured water vapour temperature and concentration in a model supersonic combustor tested in a free-piston shock tunnel facility.

The current study differs from these previous works in that it uses a different type of diode laser, the vertical-cavity surface emitting laser (VCSEL) to generate single-mode radiation at 760 nm. At these wavelengths, weak transitions in the oxygen A-band can be used for absorption measurement, allowing unseeded temperature measurements to be made in air flows. VCSELs are very small, low-power lasers that can be rapidly current-tuned over a larger wavelength range than the diode lasers used in the studies mentioned above. This allows more transitions to be accessed within a single scan, increasing the temperature sensitivity of the measurement by providing more temperature information from the flow, without the need for complex wavelength multiplexing schemes.

In this paper we present preliminary time-resolved temperature measurements obtained at measurement rates of 1–3 kHz in a shock tube flow. Initial system characterisation experiments are also presented, to determine the best-case signal-to-noise ratio of the system at lower pressures. The effect of the measurement noise is discussed, and planned improvements to the system are outlined.

Facility and Flow Conditions

The TDLAS oxygen measurements were performed in the newly commissioned ADFA shock tube facility. This facility is a shock tube of rectangular cross-section, 75 mm wide and 150 mm high. The driver section is 1366 mm long and is separated from the 5860-mm-long driven section by a 13- μ m-thick mylar diaphragm. The test section window is located 708 mm from the downstream end of the tube. Pressure is measured at two locations, 270 mm apart, with the downstream transducer 260 mm upstream of the centre of the test-section window. These two pressure measurements allow the shock speeds and post-shock pressures to be measured. The BK7 window has a diameter of 300 mm and provides optical access to the tube. The tube has flush-mounted windows, and has been specifically designed to minimise the number and strength of shock waves

generated from junctions between tube sections.

The driven section of the tube was filled with air at 96 kPa, and the driver section was filled until the mylar diaphragm burst. The shock wave speed and post-shock pressure were measured using Kistler pressure transducers with a sensitivity of 1 V/bar. The average shock speed for a single-diaphragm test was 397 ± 5 m/s. The shock wave produced when the diaphragm burst was reflected from the end-wall and proceeded past the test section again, leaving behind it a region of still higher temperature and pressure. Typical static pressure traces are presented in figure 1.

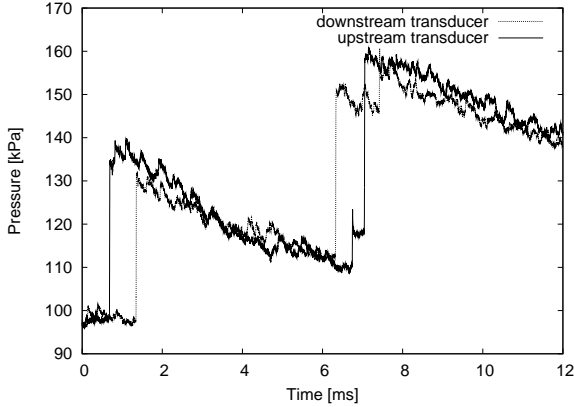


Figure 1: Typical shock tube pressure traces.

The conditions before the incident shock, after the incident shock and after the reflected shock wave have passed the test section are summarised in table 1. The temperature increases above ambient by approximately 31 K after the incident shock and by a further 32 K after the reflected shock has passed. The pressures and temperatures after the incident shock are calculated using the following equations [3]:

$$\frac{p_2}{p_1} = 1 + \frac{2\gamma}{\gamma+1} \left(\left(\frac{W}{a} \right)^2 - 1 \right) \quad (1)$$

$$\frac{T_2}{T_1} = \frac{p_2}{p_1} \left(\frac{\frac{\gamma+1}{\gamma-1} + \frac{p_2}{p_1}}{1 + \frac{\gamma+1}{\gamma-1} \frac{p_2}{p_1}} \right) \quad (2)$$

where quantities marked ₂ are after the incident shock and those marked ₁ occur before the incident shock, while W is the shock wave speed measured in the laboratory reference frame and γ is the ratio of specific heats.

The predicted pressures after the incident shock compare well with the measured pressure, as comparison of figure 1 with table 1 shows. The measured pressure after the reflected shock is lower than the predicted value, most likely because of viscous dissipation after the shock reflects from the end wall. The calculated temperatures should be within 10% of the inviscid shock calculation, based upon the difference between measured and predicted pressures.

	Temperature (K)	Pressure (kPa)
Before test	293	96
After incident shock	324	136
After reflected shock	356	191

Table 1: Calculated flow conditions for tunnel experiments.

The pressure traces in figure 1 show a second pressure rise immediately before the main reflected shock on the upstream transducer trace and approximately 1 ms after the reflected shock on the downstream transducer. This pressure rise is smaller than that of the reflected shock and moves downstream towards the end wall, passing between the two transducers as the reflected shock propagates in the other direction. This shock is not evident when the incident shock wave passes the transducers, and may be the result of non-uniform bursting of the diaphragm, generating weaker pressure disturbances that reflect along the duct after the main shock wave.

Optical Arrangement

The radiation used for these experiments is generated using an Avalon Photonics AVAP 760-SM VCSEL, whose current is controlled using a Thorlabs LDC200 current controller, modulated by a 1–3 kHz triangular waveform. The temperature of the diode is controlled using a Thorlabs TED200 temperature controller. Figure 2 shows a schematic view of the apparatus. The signal is detected using a New Focus Nirvana detector, operated in the linear difference amplifier mode, to achieve the highest bandwidth. Data is acquired from the detector at rates of 5 million samples per second for the 1-kHz data and 10 million samples per second for the 3-kHz data, producing 5000 and 3333 samples per spectrum respectively.

The light from the VCSEL is collimated using an 8-mm-focal-length aspheric lens and split into two beams, one of which passes through the test section windows of the tunnel and is reflected back by a retroreflector prism. The other beam acts as a reference beam and does not pass through the test section. Note that although in figure 2 the incoming and retroreflected beams are shown in the same horizontal plane for clarity, in the experiment the two beams are vertically displaced from each other by 10 mm and at the same horizontal location, so that the shock wave passes through both beams at the same time.

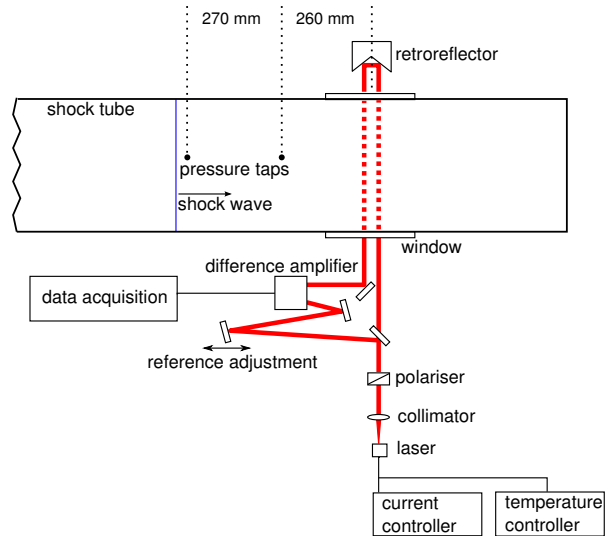


Figure 2: Experimental arrangement.

The dual-beam system in figure 2 was chosen because it allows contributions of absorption from ambient oxygen to be removed from the absorption signal in the shock tube. This is done by evacuating the tube and varying the length of the reference beam path until the contributions of laboratory air are the same, cancelling the signal. Once this has been done, all absorption in the experiments must come from the shock tube.

As seen in figure 1, approximately 6 ms elapses between the incident and reflected shock arrival at the centre of the test section. This is enough time for 5 measurements at a 1-kHz repetition rate, allowing the variation in temperature during the test to be measured. The number of measurements possible during a test is determined by the bandwidth of the detection system and the sampling rate of the data acquisition system. The limiting factor for these experiments is the detector bandwidth. The detector used had a nominal bandwidth of 125 kHz, and significant distortion in the absorption lines was noticeable for scan rates above 3 kHz. We have used a detector based upon the Texas Instruments log102 log-ratio amplifier in a previous measurement [17], but the bandwidth of that circuit was less than 45 kHz, limiting scan rates to less than 200 Hz. Although the signal-to-noise ratio is better using log-ratio detection, the maximum repetition rate was too slow for good time-resolved measurements in the shock tube flow.

The VCSEL used in these experiments can scan, by changing the diode injection current, over approximately 1 nm at wavelengths between 759 and 768 nm. The region between 760.8 and 761.6 nm is used for these tests, as it contains four oxygen transitions, including two of the three most temperature-sensitive transitions in the A-band. More than four transitions could have been chosen, but the signal-to-noise ratios of the lower-wavelength transition was not high enough, and at higher currents the laser began to produce more than one longitudinal mode.

Measurement of Temperature from Molecular Absorption

The theory of molecular absorption spectroscopy is well developed and its use for gas-phase measurements is described in detail elsewhere [9]. Absorption in the presence of resonant molecular absorption lines in a uniform gaseous medium is described by the Beer-Lambert law

$$I = I_0 e^{-k_\nu l} \quad (3)$$

where I is the intensity of absorbed light, I_0 is the intensity in the absence of absorption, l is the path length and k_ν is the absorption coefficient, which depends on the line strength and line shape according to

$$k_\nu = \int_{-\infty}^{\infty} S(T) g(\nu - \nu_0) d\nu \quad (4)$$

where g is a unity-normalised function describing the shape of the transition. S is the transition strength, and is related to the temperature T of the gas by

$$S(T) = S(T_0) \frac{Q(T_0)}{Q(T)} \exp \left[\frac{hcE}{k} \left(\frac{1}{T} - \frac{1}{T_0} \right) \right] \quad (5)$$

where Q is the partition function of the molecule, h and k are Planck's and Boltzmann's constants, c is the speed of light and E is the lower-state transition energy.

As the partition function and lower-state energy are known for the oxygen molecules and are tabulated in the HITRAN database [14], the spectrum can be precisely calculated once the temperature, pressure and concentration of molecular oxygen are known. As the shock wave is not strong enough to dissociate any of the molecular oxygen, the oxygen concentration can be assumed constant. The pressure used for the spectrum calculation is determined by the reading on the pressure transducers. The calculated spectrum is thus fitted against the measured spectrum using the temperature as a fit parameter. A nonlinear

least-squares technique is used to determine the best fit temperature. The GENSPECT adaptive line-by-line absorption code [13] was used to generate the theoretical spectra for comparison with the experimental spectra, using the measured pressure as a known input parameter to the code. A Voigt profile was used to compute the line shape g for all computed spectra, because the pressures are generally high enough for the spectra to be influenced by pressure broadening.

Processing and Fitting of Spectra

As equation 3 indicates, the log ratio of intensities is directly proportional to the path length for a given absorption coefficient k_ν . As the detector used in this study measures the difference between the two absorption signals, equation 3 can be rearranged to

$$\frac{I - I_0}{I_0} = e^{-k_\nu l} - 1 \quad (6)$$

The factor $e^{-k_\nu l} - 1$ is calculated for each iteration of the guessed temperature using equations 4 and 5, and the measurement from the difference amplifier is normalised to a separate I_0 distribution measured before each experiment. This I_0 spectrum has small dips in it due to the absorption along the reference beam path, and so the non-resonant portion of the I_0 spectrum is fitted with a third-order polynomial, which is used to normalise the measured $I - I_0$ signal obtained during the run. This step would not be necessary using the log-ratio detector, as the log-ratio detector signal is directly proportional to the absorbance along the path.

All the preparation of experimental data for fitting was performed after the experiments, using MATLAB. The background intensity modulation was removed from each spectrum by fitting a tenth-order polynomial to those portions of the spectrum not containing absorption transitions and subtracting this fitted background curve from the spectrum. This procedure was performed for each spectrum in the tunnel run, using the same wavelengths for each background fit.

The acquired spectra also need to be properly calibrated for wavelength. As the spectrum contains a number of transitions, and the variation of wavelength with current is smooth, the peak locations can be used to determine the current-wavelength calibration for the laser. Initially, the laser was characterised using a Hewlett-Packard 86120B wavelength meter. This calibration was used to determine an initial wavelength range for the spectrum. We then determined the centre wavelengths of each peak using the maximum values of the background-subtracted spectrum near each transition. At each fitting iteration, a second calibration was performed, with the wavelength of the experimental spectrum scaled so that the experimental and calculated peaks were at the same wavelength. The experimental data were then interpolated onto a regular grid, at the same sampling frequency as the computed spectrum.

We performed absorption measurements in the tube before each run, at known ambient conditions, to scale the intensity of the measured spectrum to that predicted by GENSPECT. This accounts for the gain of the detector and the concentration of oxygen molecules along the path length. The scaling factor from twenty averaged spectra was used for all temperature measurements in the subsequent shock tube experiments, allowing direct comparison between the experimental and computed spectra. It should be noted that while the experimental and computed spectra could be compared by normalising each to the area under the spectrum, this method significantly reduces the temperature sensitivity of the technique compared to calibration

at a known temperature, so we decided to use the latter method.

Results

Gas Cell Measurements

As the oxygen transitions are very weak, with line strengths at room temperature on the order of 10^{-24} cm molecule $^{-1}$, we performed initial experiments in a gas cell, to determine the best-case signal-to-noise ratios for several pressures. The gas cell had a path length of 150 mm and was filled with room-temperature air and evacuated to the required pressure by a vacuum pump. We passed the beam through the cell and measured using the difference amplifier. The effect of absorption by room temperature air was removed by equalising the path lengths with the cell fully evacuated, as mentioned previously. The nulled scan was subtracted from the scan at the required pressure, to remove any residual modulation of the absorption signal. Examples of single scans at cell pressures of 5, 10 and 20 kPa are presented in figure 3.

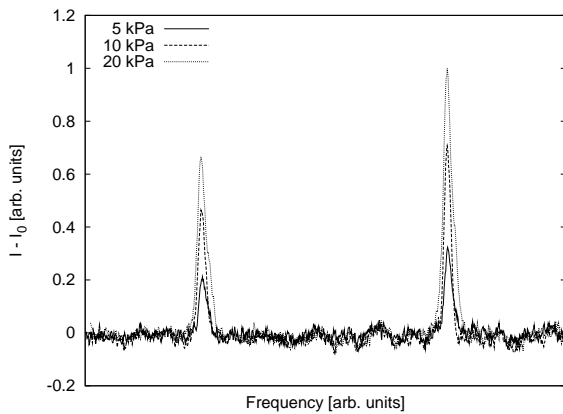


Figure 3: Absorption scans at three subatmospheric pressures.

Spectra with reasonable signal levels can be obtained at pressures as low as 5 kPa. For the three conditions shown in figure 3 the ratio of the peak signal to the standard deviation of the background varies from 18 at 5 kPa to 48 at 20 kPa. As the shock tube tests are performed at pressures in excess of 100 kPa, the signals are well above the limit of resolution of the detection system.

Shock Tube Experiments

We performed eleven experiments in the shock tube, measuring post-shock temperature in the shock tube with the tube initially filled to ambient pressure. Most of the experiments produced one or two spectra out of the three spectra between the incident and reflected shock waves. A sample post-shock fitted spectrum, with the difference between the best fit and experimental data, is shown in figure 4.

The fit for this spectrum is good, and the fitted temperature of 325 K compares well with the 324 K calculated post-shock temperature. The peak fitted values of each transition are within 5 % of the measured peaks, and this agreement is typical of the better-quality experimental data. It is apparent from the modulation of the residual curve in figure 4 that the second and third experimental and computed absorption peaks are not perfectly coincident. This is because the method used for fitting the experimental peak locations to the theoretical locations uses the maximum values of the experimental peaks as the location of the peak centre. This is not always the case, as the presence of noise can shift the peak by 1–3 sample locations either side of

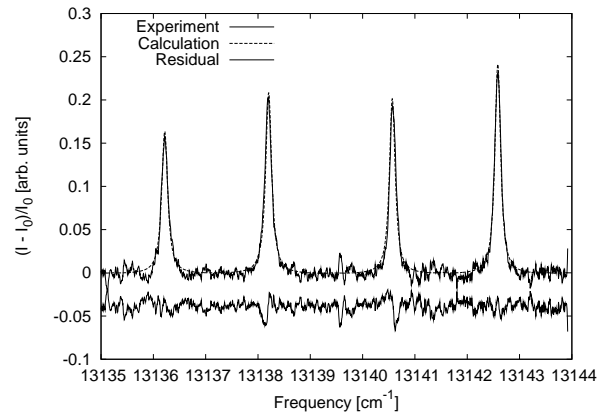


Figure 4: Sample fitted 1 kHz post-shock spectrum.

the middle of the transition. This shifting of the spectrum can bias the fit temperature for a single peak by making the fitting routine change the fit temperature to widen or thin the transition to produce a better least-squares fit. The fact that four transitions can be fitted with this laser means that this biasing effect is countered by the better-fitting data from the other transitions.

Not all of the data was of as high a quality as figure 4. Scans that occurred as the shock wave passed the test section were generally too disturbed to fit, and several of the post-shock spectra showed significant noise and DC offsets. The optical system was isolated from the shock tube, and was not sensitive to vibration of the tube as the shock was generated, so it is unlikely that mechanical vibrations alone are responsible for this disturbance to the measured spectra. We believe that this effect was due to movement of the test section windows during the experiment. The test section windows were mounted using o-rings, and the passage of the shock causes a small displacement of the window. This displacement changes the light path between the signal and reference beams of the system, causing a modulation of the signal that can be significant when compared to the very small absorbances being measured. The 3-mm-diameter photodiodes used in the detector were not much larger than the beam itself, so even a small deviation in the signal beam could have a significant effect by the time the beam reaches the detector. Only a few spectra obtained after the reflected shock wave were of sufficiently high quality to be fitted at all, which indicates that the effect is more pronounced at the higher pressure. As the system was aligned at atmospheric pressure, this is not surprising.

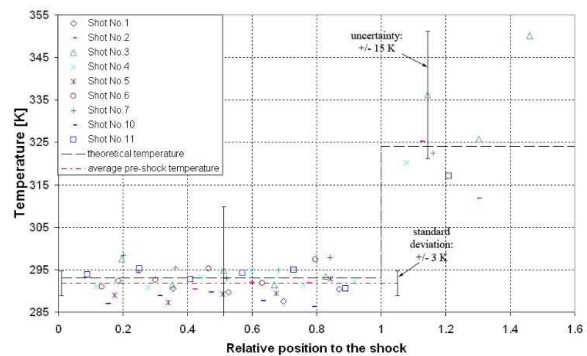


Figure 5: Summary of pre-shock and post-shock temperature measurements.

Figure 5 collects all of the good quality pre-shock and post-

shock temperature data for the 11 tunnel runs investigated at these conditions. With the exception of one possible outlier during the third run, the post-shock results are consistent. The pre-shock temperature measurements agree to within ± 3 K, which is an indication of the uncertainty of the technique under near-ideal conditions. Based upon the small sample of post-shock measurements we estimate a temperature uncertainty of ± 15 K.

Given these results, the main cause of experimental error in these measurements is deflection of the signal beam caused by a combination of density gradients in the flow and movement of the windows as the shock passes. As the path length between the first test section window and the detector is more than 1 m and the diameter of the silicon detectors is only 3 mm, the deflection of the beam can have a significant effect on the measured signal through increased DC offset and the formation of etalon fringes caused by small changes in path length between the two beams and through vignetting of the signal beam on the photodetector.

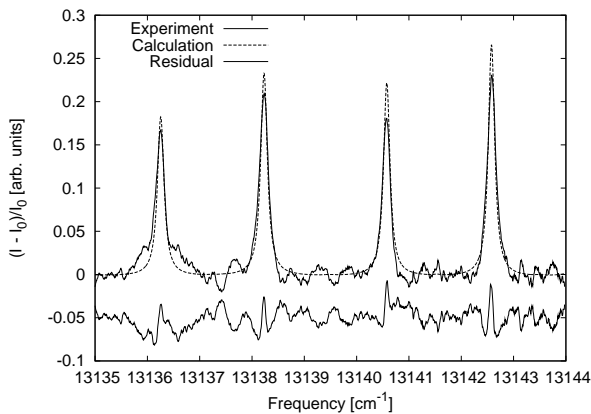


Figure 6: Sample fitted 3 kHz post-shock spectrum.

Some additional measurements were performed at the higher scan rate of 3 kHz. One such spectrum is shown in figure 6. In addition to being noisier, the peaks in figure 4 are broader and slightly asymmetric, which has the effect of reducing the fit at the peaks and causing the fitting routine to fit to systematically low temperatures. The fitted temperature for the spectrum in figure 6 is 300 K, significantly lower than the 1 kHz fitted temperature and the predicted post-shock temperature in table 1.

The systematically low fit temperature at the 3 kHz scan rate is consistent over several spectra, and is caused by reaching the 125 kHz bandwidth limit of the detector. This behaviour is noticeable at even lower frequencies when a log-ratio detector is used. The log-ratio detector described in reference [17] has been tested in room air at various scan rates, and the variation in measured temperature with scan frequency is shown in figure 7. In this plot, the error bars indicate \pm one standard deviation in fitted temperature over ten measurements.

The maximum bandwidth of the log-ratio detector used to produce figure 7 is 45 kHz, so the measured temperature starts to decrease at a rate between 150 and 300 Hz. The trend of lower fitted temperature at higher scan rates is clear, and similar to that seen when comparing the 1 kHz and 3 kHz tunnel tests.

Conclusions and Future Work

This paper presents a successful measurement of post-shock temperature in a shock tube facility at a measurement rate of 1 kHz. The measured temperature is consistent with the prediction of a 1-dimensional, inviscid calculation, but the acquired

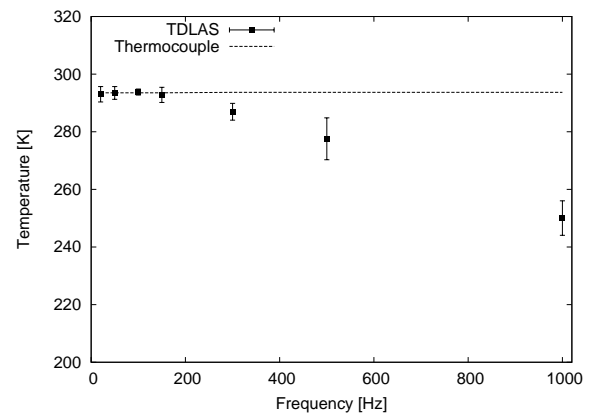


Figure 7: Effect of scan rate on measured temperature for a log-ratio amplifier.

measurements were not sufficient for a statistically significant uncertainty in post-shock temperature. Only around 30 % of the post-shock scans were of high enough quality to be fitted, while nearly all of the post-reflected-shock scans were not of high-enough quality to be fitted. Those that were able to be fitted gave temperatures within 15 K of the predicted values.

Despite these encouraging initial results, there are two obstacles that need to be overcome to make the technique capable of producing consistent and accurate temperature measurements: movement of the windows providing optical access to the test section and steering of the signal beam by density gradients in the flow. Using hard-mounted windows, larger photodiodes and keeping the path length of the system as small as possible should all assist in improving the stability of the system to the ± 3 K measured for the pre-shock spectra. The scale of the temperature increases in this shock tube should be no more than 100 K above ambient, and the sensitivity of the technique itself should not decrease significantly over this temperature range.

One other obvious improvement to the experiment involves increasing the bandwidth of the detection system. We are currently performing experiments using a faster log-ratio amplifier with a bandwidth of 5 MHz. This should be sufficient for scan rates close to 10 kHz — fast enough for both shock tube and shock tunnel configurations. The log-ratio detector is also better at cancelling common-mode noise [2] and does not require a separate measurement of I_0 , making it a much better option for these experiments provided the higher measurement bandwidth can be assured.

Acknowledgements

This work was funded by a University of New South Wales special research grant, and this support is gratefully acknowledged.

References

- [1] Allen, M., Diode laser absorption sensors for gasdynamic and combustion flows, *Measurement Science and Technology*, **9**, 1998, 545–562.
- [2] Allen, M., Carleton, K., Davis, S., Kessler, W., Otis, C., Palombo, D. and Sonnenfroh, D., Ultrasensitive dual-beam absorption spectroscopy: Applications for near-infrared and visible diode lasers, *Applied Optics*, **34**, 1995, 3240–3249.

- [3] Anderson, J. D., *Modern Compressible flow with Historical Perspective*, McGraw-Hill, 1990, 2nd edition.
- [4] Boyce, R. R., Pulford, D. R. N., Houwing, A. F. P. and Mundt, C., Measurements using CARS in a hypervelocity shock layer flow and comparisons with CFD calculations, *Shock Waves*, **6**, 1996, 41–51.
- [5] Danehy, P. M., Mere, P., Gaston, M. J., O’Byrne, S., Palma, P. C. and Houwing, A. F. P., Fluorescence measurement of the velocity-field produced by the hypersonic separated flow over a cone, *AIAA Journal*, **39**, 2001b, 1320–1328.
- [6] Griffiths, A. D. and Houwing, A., Diode laser absorption spectroscopy of water vapor in a scramjet combustor, *Applied Optics*, **44**, 2005, 6653–6659.
- [7] Hanson, R. K., Advanced laser diagnostics for reactive flows, in *AIAA paper 2002-0196*, 2002.
- [8] Matsuda, A., Fujita, K., Sato, S. and Abe, T., Absorption spectroscopy for temperature measurement behind shock wave at super-orbital velocity, *Journal of Thermophysics and Heat Transfer*, **19**, 2005, 294–299.
- [9] Measures, R. M., *Laser Remote Chemical Analysis*, Wiley, 1988.
- [10] O’Byrne, S., Danehy, P. M. and Houwing, A. F. P., Non-intrusive temperature and velocity measurements in a hypersonic nozzle flow, in *The Proceedings of the 22nd AIAA Aerodynamic Measurement Technology and Ground Testing Conference, St Louis, MI, USA*, 2002, AIAA 2002-2917.
- [11] O’Byrne, S., Danehy, P. M. and Houwing, A. F. P., Investigation of hypersonic nozzle flow uniformity using NO fluorescence, *Shock Waves*, **15**, 2006, 81–87.
- [12] Palma, P. C., Danehy, P. M. and Houwing, A. F. P., Non-intrusive thermometry in shock layers using multi-line fluorescence imaging, *Shock Waves*, **3**, 1997, 49–53.
- [13] Quine, B. M. and Drummond, J. R., Genspect: a line-by-line code with selectable interpolation error tolerance, *Journal of Quantitative Spectroscopy and Radiative Transfer*.
- [14] Rothman, L. S., Jacquemart, D., Barbe, A., Benner, D. C., Birk, M., Brown, L., Carleer, M. and *et al.*, C. C., The HITRAN 2004 molecular spectroscopic database, *Journal of Quantitative Spectroscopy and Radiative Transfer*, **96**, 2005, 139–204.
- [15] Thurow, B., Jiang, N., Samimy, M. and Lempert, W., Narrow-linewidth megahertz-rate pulse-burst laser for high-speed flow diagnostics., *Applied Optics*, **43**, 2004, 5064–5073.
- [16] Trinks, O. and Beck, W. H., Application of a diode-laser absorption technique with the D₂ transition of atomic Rb for hypersonic flow-field measurements., *Applied Optics*, **37**, 1998, 7070–7075.
- [17] Webster, L., O’Byrne, S. and Houwing, A., Determination of temperature distributions in air using a scanning vertical-cavity surface-emitting laser, in *Proceedings of the 4th Australasian Conference on Laser Diagnostics in Fluids Mechanics and Combustion*, 2005.
- [18] Wehe, S. D., Baer, D. S. and Hanson, R. K., Tunable diode-laser absorption measurements of temperature, velocity and H₂O in hypervelocity flows, in *AIAA-97-3267*, 1997.